JOURNAL OF APPLIED CRYSTALLOGRAPHY
ISSN 1600-5767

Effect of phenol red dye on monocrystal growth, crystalline perfection, and optical and dielectric properties of zinc (tris) thiourea sulfate

Mohd. Shkir,[a]* V. Ganesh,[a] S. AlFaify,[a]* K. K. Maurya[b] and N. Vijayan[b]

[a]Advanced Functional Materials and Optoelectronic Laboratory (AFMOL), Department of Physics, King Khalid University, PO Box 9004, Abha, 61413, Saudi Arabia, and [b]National Physical Laboratory, Council of Scientific and Industrial Research, Dr K. S. Krishnan Road, New Delhi, 110012, India. *Correspondence e-mail: shkirphysics@gmail.com, shkirphysics@kku.edu.sa, sasaalfaify@hotmail.com

Received 6 June 2017
Accepted 4 October 2017

Edited by G. Kostorz, ETH Zurich, Switzerland

Keywords: phenol red dye; crystal growth; FT-Raman spectroscopy; scanning electron microscopy; SEM; optical properties; dielectric response; photoluminescence.

In this work, the growth of large size (~25 × 29 × 5 mm and ~25 × 24 × 6 mm) colorful single crystals of zinc (tris) thiourea sulfate (ZTS) in the presence of 0.05–2 wt% phenol red (PR) dye was achieved using a simple and low-cost technique. Powder X-ray diffraction patterns confirm the presence of PR dye, which is indicated by an enhancement of the Raman peak intensities, a shift in their position and the appearance of a few extra peaks. The quality of the grown crystals was assessed by high-resolution X-ray diffraction, which shows that the crystalline perfection of 1 wt% PR-dyed ZTS crystals is better than that of 2 wt% PR-dyed crystals. The measured UV–vis absorbance spectra show two additional, strong absorption bands at ~430 and 558 nm in the dyed crystals, due to the presence of PR dye, along with a band at ~276 nm which is present for all crystals but is slightly shifted for the dyed crystals. Photoluminescence spectra were recorded at two excitation wavelengths (λ_{exc} = 310 and 385 nm). The luminescence intensity is found to be enriched in dyed crystals, with some extra emission bands. An enhancement in the value of the dielectric constant and a.c. electrical conductivity was also observed in the dyed ZTS crystals.

1. Introduction

Recently, nonlinear optical (NLO) materials have been found to have important applications in, for example, opto-electronic, photonic, data conversion, retrieval, storage and frequency-doubling devices (Saleh & Teich, 1991; Penn *et al.*, 1991; Shakir *et al.*, 2009; Shakir, Kushwaha *et al.*, 2010; Shkir, Abbas *et al.*, 2014; Shkir, AlFaify *et al.*, 2015; Badan *et al.*, 1993; Zaitseva & Carman, 2001; Shkir, Muhammad, AlFaify *et al.*, 2015; Shkir, Muhammad & AlFaify, 2015). Luminescent dyed crystals exhibit better properties than polymers and glasses as they possess superior thermal conductivity, low dispersion and intrinsic polarization, have fewer defects, and can be used in laser devices (Yang & Ozin, 2000, Wanke *et al.*, 1997). Benedict *et al.* (2003) studied dying processes in crystals. A review on dyeing of different crystal faces has also been published recently (Kahr & Shtukenberg, 2016; Kahr & Gurney, 2001).

Zinc (tris) thiourea sulfate (ZTS) single crystals have good NLO properties compared to standard NLO materials such as potassium dihydrogen phosphate (Dhumane *et al.*, 2008). Having such a key characteristic, ZTS is a valuable component in high-energy lasers as a frequency convertor. Recently, the growth of dyed ZTS crystals has been reported; the grown crystals had modified physical properties that make them suitable for linear, nonlinear and piezoelectric applications (Bhandari *et al.*, 2014; Shkir, 2016; Shkir *et al.*, 2016). These

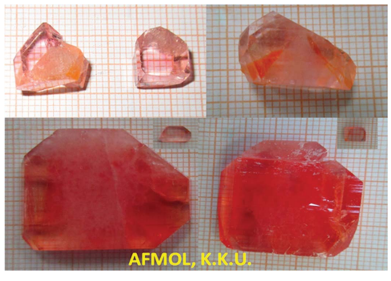

results show that the properties of ZTS crystals are strongly affected when they are grown in the presence of dye or with dye doping.

Phenol red (PR) is well known as a pH indicator, usually applied in cell culture, and has a wide range of applications (Berthois *et al.*, 1986; Mills & Skinner, 2011). According to the current available literature, there have been no reports on ZTS crystal growth in the presence of PR dye so far. In the present work, our aim is to grow good quality colorful single crystals of ZTS with different concentrations of PR dye, which we denote as PRZTS. The pH value of all the prepared solutions for crystal growth was measured. Furthermore, the grown crystals were subjected to X-ray diffraction and FT-Raman analyses to confirm structural and vibrational changes, respectively, high-resolution X-ray diffraction (HRXRD) to assess the crystalline perfection, UV-vis spectroscopy for band gap analysis, photoluminescence (PL) spectroscopy to study the fluorescence behavior, and dielectric and mechanical studies to discern the defects and strength of the grown crystals.

2. Experimental

2.1. Synthesis and crystal growth

High-purity zinc sulfate heptahydrate ($ZnSO_4{\cdot}7H_2O$), thiourea [$CS(NH_2)_2$] and PR dye were purchased from Sigma-Aldrich. $ZnSO_4{\cdot}7H_2O$ and $CS(NH_2)_2$ in a 1:3 ratio were dissolved in two different beakers containing double distilled (DD) water. Pure ZTS $\{Zn[CS(NH_2)_2]_3{\cdot}SO_4\}$ was synthesized by mixing the two solutions in another beaker using a temperature-controlled magnetic stirrer (Isotemp, Fisher Scientific) above room temperature (*i.e.* 323 ± 1 K). The chemical reaction between these two species to obtain the final product is

$$ZnSO_4{\cdot}7H_2O + 3CS(NH_2)_2 \rightarrow Zn[CS(NH_2)_2]_3{\cdot}SO_4.$$

A similar procedure was followed to prepare another four sets of ZTS solution, to which were added different concentrations of PR dye, from 0.05 to 2 wt% (*i.e.* from 0.0036 to 0.146 g). The solutions were again mixed thoroughly by regular stirring (700 r min^{-1}) for 24 h at the same temperature and red solutions were obtained as a result of the dye. The pH of all the prepared solutions was measured using a pH meter, and the variation of pH with PR dye content is shown in Fig. 1(*a*). It can be concluded that the pH is strongly affected by the addition of dye to the parent solution.

All the prepared solutions were left at the same temperature to evaporate the solvent and obtain the salts of the pure and dyed ZTS which were further used for single-crystal growth. Again, the synthesized materials were dissolved in DD water at the same temperature with the aim of growing good quality single crystals. The temperature was reduced to 300 ± 1 K in steps of 1 K per 12 h and the solution was carefully watched. It was found that on reducing the temperature nucleates were formed, and these were dissolved by adding an appropriate amount of DD water. Finally the prepared saturated solutions were filtered using filter paper into new beakers. All of the beakers were then covered with a pierced lid and kept in a constant temperature bath at 300 ± 1 K. The solutions were observed frequently to avoid any multiple nucleations. Fig. 1 shows examples of the grown crystals of pure ZTS [see the inset of Fig. 1(*a*)] and ZTS with 0.05, 0.1, 1 and 2 wt% PR dye addition, respectively (Fig. 1*b*, i–iv). It is clear that the pure crystal is transparent white; however, in the presence of dye the crystal becomes colored. The crystals shown in Fig. 1 were harvested from their respective solutions after about 60 d. The size of the grown crystals with 1 wt% dye is ~25 × 29 × 5 mm and with 2 wt% dye is ~2 × 24 × 6 mm. From the figure it is also clear that the dye is homogeneously adsorbed in the ZTS crystals at higher concentrations and the morphology is greatly modified. From the insets of Figs. 1(*a*) and 1(*b*), it is clear that the faces such as (100), (001), (101), (011), (011) and (010) present in the pure ZTS crystal (Fig. 1*a*) are suppressed as a result of the presence of the dye and growth is taking place along the [110] direction. For further studies, we have chosen the crystals grown at higher dye concentrations (*i.e.* 1 and 2 wt%) along with the pure crystal.

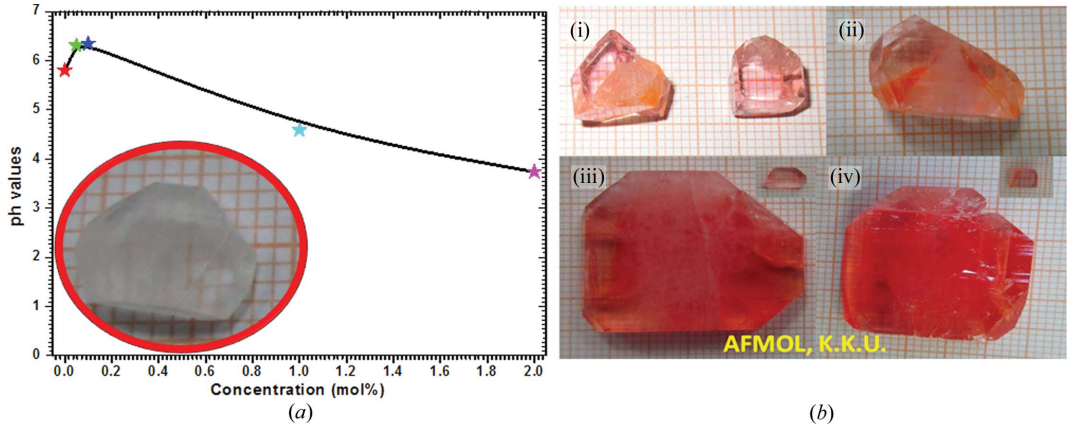

(*a*) (*b*)

Figure 1
(*a*) Variation of pH values and (*b*) as-grown single crystals of ZTS with (i) 0.05 wt%, (ii) 0.10 wt%, (iii) 1 wt% and (iv) 2 wt% PR dye.

2.2. Characterization methods

Some of the grown ZTS and PRZTS crystals were crushed to fine powders for ∼5 min and used to record powder X-ray diffraction patterns using a Shimadzu (Japan) XRD-6000 powder X-ray diffractometer with Cu $K\alpha$ radiation, λ = 0.1543 nm, operated at 40 kV, 30 mA at a scan rate of 0.2° m^{-1} over an angular range of 5–70° at 300 K. As-grown crystals [shown in the insets of Figs. 1(*a*) and 1(*b*) were used to record the FT-Raman spectra on a Thermo Scientific DXR FT-Raman spectrometer in the wavenumber range of 3500–50 cm^{-1}. The crystalline perfection was assessed by HRXRD (PANalytical X'Pert PRO MRD system) using Cu $K\alpha_1$ radiation (λ = 1.540598 Å). Scanning electron microscopy (SEM) (JSM 6360 LA, JEOL Ltd, Tokyo, Japan) was used to record the surface topography. UV–vis absorbance spectra were measured using a JASCO 570 UV–vis–NIR spectrophotometer in the wavelength range from 190 to 1000 nm. A Thermo Fisher Scientific Lumina fluorescence spectrometer was used to record the PL spectra in the wavelength range of 380–700 nm at 300 K. The dielectric and a.c. electrical conductivity measurement was done in a high frequency range using a Keithley 4200-SCS system at 300 K.

3. Results and discussion

3.1. Structural studies

Fig. 2(*a*) shows measured X-ray diffraction patterns for the pure PR dye, pure ZTS and dyed ZTS powdered specimens. It is clear from the figure that the intensity of the diffraction peaks has been increased because of the dye, which indicates the good crystalline quality of the dyed crystals. On comparing the diffraction patterns of the pure dye and the pure and dyed ZTS crystals it is observed that there are some extra peaks in the patterns of the dyed crystals along with some shifting in the peaks' positions (see Fig. 2*b*). The extra peaks observed at 13.08° (021), 18.49° (212), 21.25° (321), 24.54° (322) and 31.24° (432) are due to the presence of the PR dye (JCPDS No. 1224041) in the ZTS crystals (see Fig. 2*b*). The intensity of the 211, 406 and 617 peaks is found to be particularly enhanced for 2 wt% PR-dyed ZTS crystals. For the confirmation of the crystal system and lattice parameter calculations, the recorded XRD data were used for refinement in the *CHECKCELL* software (Laugier & Bochu, 2000). The peak positions were determined by basic data processing using the XRD-6000 software (Shimadzu, Kyoto, Japan) and high-intensity peaks were used as input in the above-mentioned software to obtain accurate refined parameters. The number of peaks is found to be increased in the dyed crystals. The refinement confirms that the grown crystals have orthorhombic crystal structure with space and point groups of $Pca2_1$ and $mm2$, respectively. The refined lattice parameters are presented in Table 1 and are found to be in close agreement with previously reported values (Andreetti *et al.*, 1968; Ushasree, Jayavel & Ramasamy, 1999; Ushasree, Jayavel, Subramanian & Ramasamy, 1999; Moitra & Kar, 2007; Cole & Hickstein 2013). It can be seen from Table 1 that the lattice parameters vary with PR concentration.

Table 1
Refined lattice parameters of pure and dyed ZTS crystals.

	Previous work†	Current work‡		
Lattice parameters	ZTS	ZTS	PRZTS (1 wt%)	PRZTS (2 wt%)
a (Å)	11.0673	11.0607	11.0812	11.0809
b (Å)	7.7342	7.7331	7.7366	7.7516
c (Å)	15.5573	15.5741	15.5521	15.5454
V (Å^3)	1331.65	1332.10	1333.29	1335.264

† Cole & Hickstein (2013). ‡ Refined by *CHECKCELL*.

3.2. Vibrational (FT-Raman and FT-IR spectroscopy) studies

The measured FT-Raman spectra of the ZTS and PRZTS crystals in the characteristic wavenumber range are shown in Fig. 3(*a*). It is seen that the Raman intensity and transparency are significantly increased in the ZTS crystals grown in the presence of dye. This indicates an enhancement in fluorescence activity of PRZTS crystals. The FT-Raman spectrum for the higher wavenumber range is not shown here; however, all

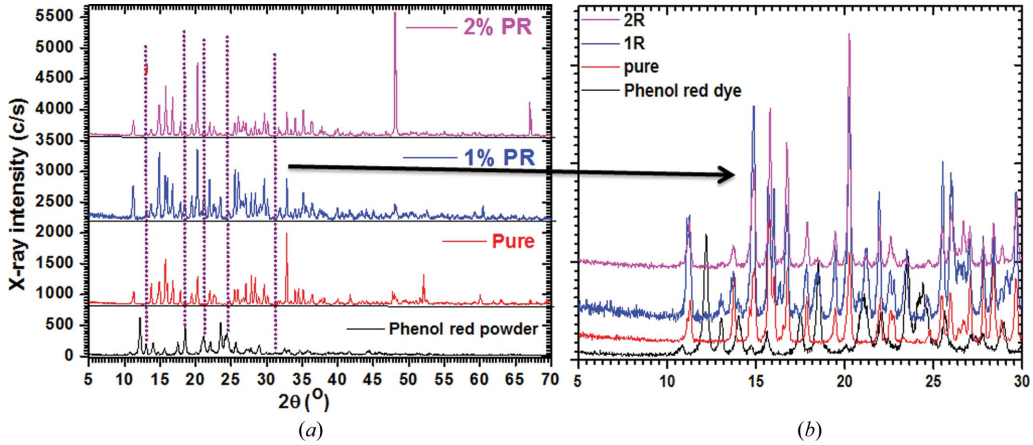

Figure 2
(*a*) Powder X-ray diffraction patterns and (*b*) close-up view in the angular range of 5–30°.

Table 2
Observed vibrational modes (FT-Raman) and their corresponding assignments.

Observed wavenumbers (cm^{-1})			
ZTS	PRZTS (1 wt%)	PRZTS (2 wt%)	Assignments
96, 66, 50, 35, 24	92, 64, 45, 37	95, 65, 47, 33, 23	Lattice vibration
152, 125, 110	150, 123, 111	151, 124, 110	Lattice vibration
238	234	235	Lattice vibration
265	262	261	Zn—S
430	431	429	$\upsilon(SO_4)$
485	480	483	Vibration (Zn—S), (Zn—O)
530	514, 533	525, 546	υ(Zn—O)
592, 602	605	595	$\upsilon(SO_4)$
715	711	713	υ(C—N), υ_s(C═S)
953	955	951	$\upsilon(SO_4)$
1027	1037	1026	S═C—N
1090	1088	1089	$\rho(NH_2)$
1109	1108	1111	$\upsilon(SO_4)$
1408	1395	1404	υ_{as}(CS)
1438	1435	1440	υ_{as}(CS), υ_{as}(CN)
1513	1514	1512	υ_{as}(CN), S═C—N, N—C—N
1633, 1651	1643, 1661	1645, 1667	$\delta(NH_2)$
3213	3211	3208	$\upsilon_s(NH_2)$
3351	3342, 3390	3340	$\upsilon_{as}(NH_2)$

the bands observed in this range can be assigned to symmetric and asymmetric vibrations of NH stretching of several N—H···O bonds in the ZTS with minute shifts due to the presence of the dye. The vibrational modes for the ZTS and PRZTS crystals are presented in Table 2. Raman modes at ∼1513, 1438 and 1408 cm^{-1} in ZTS occur because of stretching and asymmetric stretching vibrations of N—C—N and C═S bonds, respectively (Venkataramanan *et al.*, 1994). However, these bands are found to be shifted in the dyed crystals (see Table 2). The vibration bands at 1408 and 715 cm^{-1} arise from metal–sulfur bonding of zinc with thiourea. The positions of these bands in the dyed crystals are also found to be shifted, as can be seen from Table 2. These bands are in good correlation with earlier reports (Venkataramanan *et al.*, 1994). The bands due to stretching and rocking vibrations of SO_4 and NH_2 are seen at ∼1109, 953, 602, 430 and 1090 cm^{-1}, respectively, in ZTS, but these bands are clearly shifted in the dyed crystals. The Raman band at 1027 cm^{-1} is due to S═C—N vibrations. Raman bands due to symmetric stretching and rocking vibrations of C═S and C—N mode occur at ∼715 and 485 cm^{-1} in ZTS and show a clear shift in position for PRZTS crystals (see Table 2). The band due to stretching vibration of the Zn—S bond is seen at 265 cm^{-1} in ZTS, but is also shifted in the PRZTS crystals (Venkataramanan *et al.*, 1994). The other vibrational modes listed in Table 2 are due to lattice vibrations in ZTS, and these are also seen in PRZTS with a shift in their positions. The shift in peak positions shows that there is a clear interaction between the dye and ZTS, which is also confirmed by the color of the crystals (see Fig. 1) and the XRD study. The bands due to the presence of dye are not quite detectable by the Raman laser instrument owing to the low concentration of the dye, but they may be identified by surface-enhanced FT-Raman spectroscopy.

Furthermore, we have recorded FT-IR spectra for ZTS and PRZTS to see the effect of the dye on the vibrational modes, as shown in Fig. 3(*b*). It can be clearly seen in the figure that all the grown crystals have similar vibrational frequencies (Bhandari *et al.*, 2014; Shkir, 2016; Selvapandiyan *et al.*, 2013). However, some new bands, as well as band shifts, were observed in the dyed crystals. The strong band due to plane bending of the NH_2 group which occurs at 1632 cm^{-1} in ZTS is found to be shifted to 1628 and 1627 cm^{-1} in 1 and 2 wt% PRZTS crystals. The band due to stretching vibration of the N—C—N bond which is observed at 1517 cm^{-1} in ZTS is found to be shifted to 1511 and 1507 cm^{-1} in the PRZTS crystals. The band due to stretching vibration of SO_4 which occurs at 1128 cm^{-1} in ZTS is shifted to 1127 and 1107 cm^{-1} in the respective PRZTS crystals. The band observed at 1090 cm^{-1} in ZTS becomes more broad and seems to disappear in the dyed crystals. The band observed at 1031 cm^{-1} in ZTS is shifted to 1030 and 1021 cm^{-1} in the respective dyed crystals. The band due to SO_4 at 590 cm^{-1} in ZTS is observed to be at 581 and 577 cm^{-1} in the respective dyed crystals. A very broad low-intensity vibrational band at 1470 cm^{-1} was observed, and this may be assigned to stretching vibration of

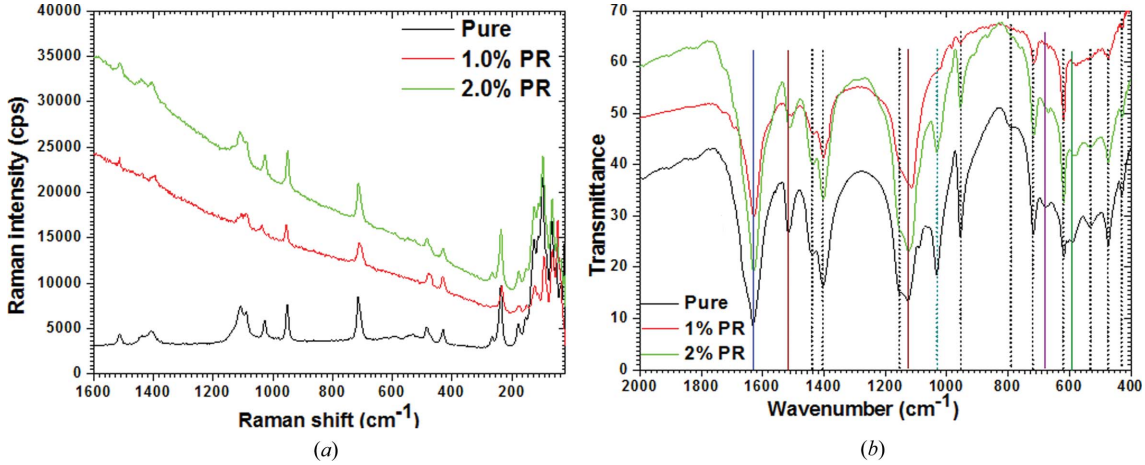

(*a*) (*b*)

Figure 3
(*a*) FT-Raman and (*b*) FT-IR spectra of ZTS and PRZTS crystals.

the sulfonate group of the PR dye (which is seen at ~1460 cm^{-1} in the pure dye) (Wahab & Hussain, 2016). This band is not easily visible in the current spectra. However, by zooming in on the specific range of the spectra it can be found. A new broad and sharp vibrational band observed at 982 cm^{-1} in the PRZTS crystals may be due to the PR dye. However, this band has been reported in pure PR at 1016 cm^{-1} (Wahab & Hussain, 2016). The other two new bands at 866 and 908 cm^{-1} that are observed in the dyed crystals may also be due to the PR dye, as these bands in the pure dye are reported at 862/840 and 919/912 cm^{-1} (Wahab & Hussain, 2016). The occurrence of these bands provides clear evidence of the dye in the ZTS crystals.

3.3. Surface topography study by SEM

Capturing the surface topography using SEM can help us to assess the quality of the grown crystals to some extent. SEM images for as-grown single crystals and their surface topographs at lower and higher resolution are shown in Fig. 4. It can be seen that the surface morphology of ZTS has been modified by the PR dye compared to the pure crystals reported in our previous studies (Shkir, 2016). The SEM images clearly indicate that the dye has been adsorbed on the surface of the ZTS crystals. The surface of the 2 wt% PR-dyed crystal is clearly affected compared to the 1 wt% PR-dyed crystal. The 2 wt%-dyed crystal surface contains etch-pit-like structures on the surface when we test the surface at low scale, which are not present in the 1 wt%-dyed crystals at the same scale. This shows that the surfaces of the ZTS crystals grown in the presence of higher dye concentrations are more affected than those grown at low concentrations.

3.4. High-resolution X-ray diffraction studies

The HRXRD diffraction curves for the (200) diffraction planes of pure and 1 and 2 wt% PR-dyed ZTS crystals are shown in Fig. 5. The curve in Fig. 5(*a*) is quite sharp and possess a single peak with a very low full width at half-maximum (FWHM) of the order of 8″, which is quite close to that expected for an ideally perfect single crystal according to the dynamical theory of X-ray diffraction (Batterman & Cole, 1964; Shakir, Kushawaha *et al.*, 2010). The sharp nature of the intensity *versus* glancing angle curve shows that this crystal contains a very low density of point defects and their agglomerates. On very close observation of the curve, there is a slight asymmetry between the negative and positive sides with respect to the exact Bragg peak position (comparison curve is not shown), which indicates that the ZTS crystal predominantly contains vacancy-type defects. The same has been reported previously (Kushwaha *et al.*, 2011). However, the value of FWHM reported here for the pure ZTS crystal is slightly less than the earlier reported value (Kushwaha *et al.*, 2011). The low value of FWHM indicates the better crystalline perfection of the single crystals reported in the current work, which directly indicates better growth conditions. Fig. 5(*b*) shows the diffraction curve of the 1 wt% PR-dyed ZTS crystal, which is broader than that of the pure ZTS crystal. The presence of PR has yielded a significant increase in the FWHM value, from 8 to 19″, and clear asymmetry caused by increased intensity on the negative side. The asymmetry is clearly visible since the broadening of the overall diffraction curve has been increased owing to the inclusion of the PR dye in the ZTS lattice. This diffraction curve clearly shows the presence of predominantly vacancy defects in the 1 wt% PR-dyed ZTS crystal. The higher concentration of 2 wt% PR dye leads to a more symmetric and broader diffraction curve, having an FWHM value of 84″ (Fig. 5*a*). Although this curve looks very symmetric in nature, towards the positive side the scattering intensity is much higher compared to the negative side, which is due to the presence of a grain boundary. The grain boundary is separated by ~763″ from the main peak (see Fig. 5*c*). The appearance of this grain boundary at 2 wt% PR

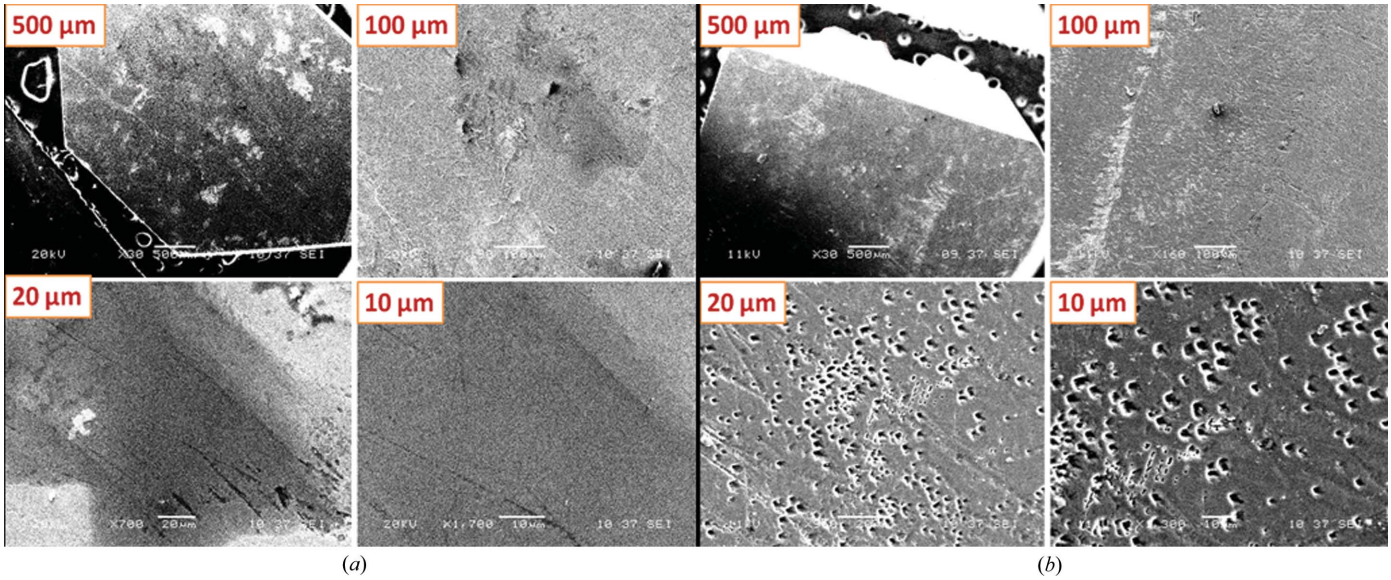

(*a*) (*b*)

Figure 4
SEM topographs of (*a*) 1 wt% and (*b*) 2 wt% PRZTS single crystals.

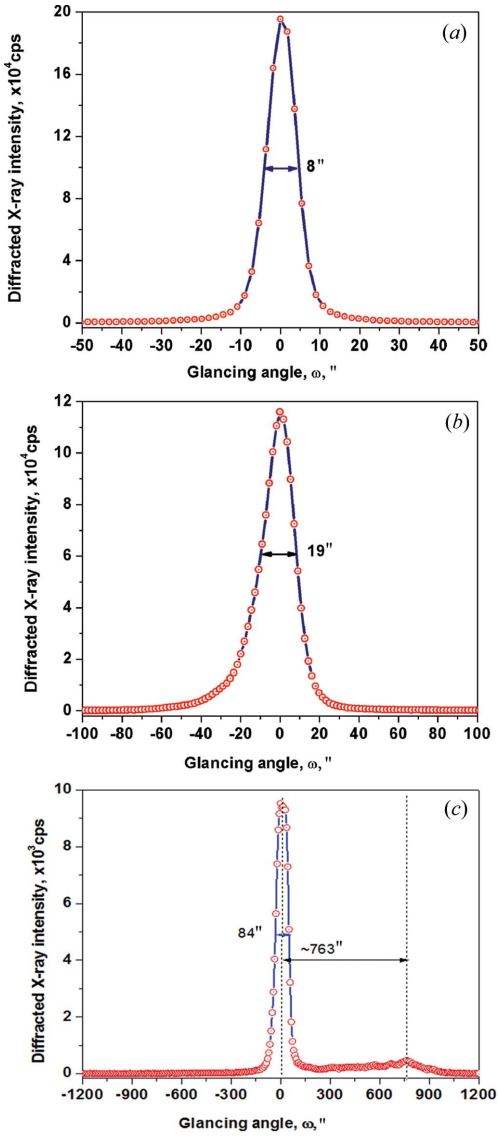

Figure 5
HRXRD diffraction curves for (*a*) pure, (*b*) 1 wt% PR-dyed and (*c*) 2 wt% PR-dyed ZTS single crystals.

dye concentration indicates the upper limit of possible interaction of PR dye in ZTS crystals.

3.5. UV–visible spectroscopy analysis

To establish the effect of the dye on the grown crystals' optical applications, we measured absorbance spectra from colloidal solutions of the crystals in double distilled water, as shown in Fig. 6(*a*). It can be seen from the figure that all the grown crystals of ZTS show much less absorbance in the wavelength range of 300−1000 nm. However, the dyed crystals have peaks in their spectra in the wavelength range of 600–1000 nm. This indicates that the grown crystals can be used in particular wavelength ranges in optoelectronic devices. In the pure and 1 and 2 wt%-dyed ZTS crystals absorption bands are observed at 276, 274 and 272 nm, respectively. However, two more absorption bands with strong absorption values are observed at 430 ± 2 and 558 ± 2 nm in both PRZTS crystals. These bands are due to the presence of the PR dye and are shifted in comparison to the spectrum of the pure PR dye (Rovati *et al.*, 2012). These bands clearly show that the dye has a very strong effect on the ZTS crystalline matrix.

Furthermore, the optical band gap was calculated from the Tauc plot for the ZTS and PRZTS crystals. For energy gap calculation first we calculated the absorption coefficient α using the well known Beer–Lambert law relation, $\alpha = 2.303A/R$, where A is the UV–vis absorbance and R is the path length of the quartz cuvette (10 mm) used during the measurement. The Tauc plots for PRZTS crystals are shown in Fig. 6(*b*). The value of α for the pure ZTS crystal is found to be ∼0.02. However, in the dyed crystals this value is significantly increased and it is found to be ∼0.14 and 0.17 at ∼194 nm wavelength. To evaluate the energy gap we have extrapolated a straight line from the $(\alpha h\nu)^2$ *versus* $h\nu$ curve to the point of intersection with the $x(h\nu)$ axis (Fig. 6*b*). The value of the energy gap is found to be 4.32, 4.29 and 4.25 eV for ZTS and 1 and 2 wt%-dyed PRZTS crystals, respectively. The energy gap value is found to be reduced in the dyed crystals compared to the pure crystal, which is a clear indication of dye interaction

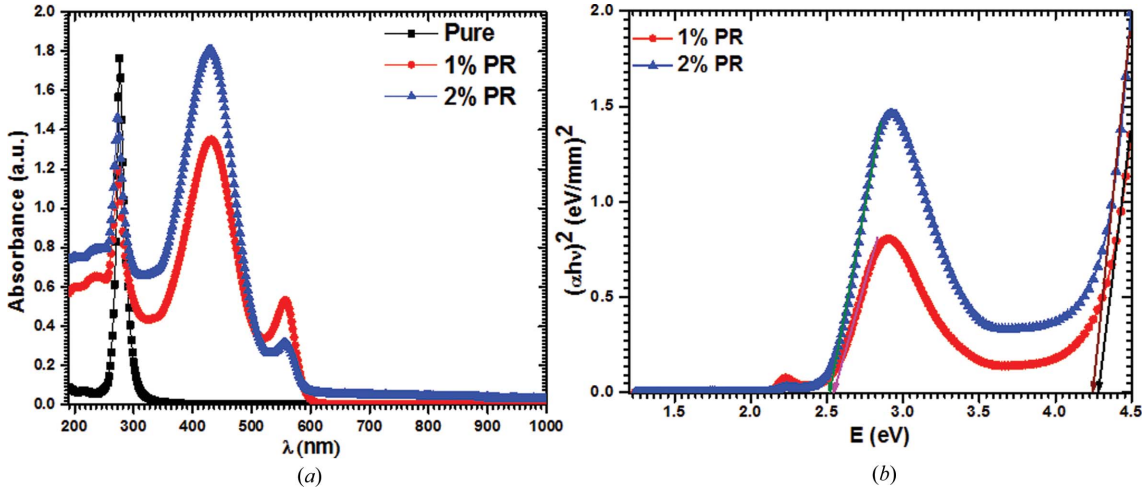

Figure 6
(*a*) Absorbance spectra and (*b*) energy gap plots for ZTS and PRZTS crystals.

with the ZTS matrix. Such a reduction in energy gap has also been calculated from diffuse reflectance (DR) data for powdered specimens of dyed ZTS crystals (Shkir *et al.*, 2016; Shkir, 2016). However, the value of the energy gap is found to be lower compared to our previous reports in which these values were calculated using DR data by the Kubelka–Munk method (Shkir *et al.*, 2016; Shkir, 2016). The band gap values for pure and dyed ZTS crystals have also been reported to be 4.16–4.18, 4.046, 4.1818—4.1995 and 4.54 eV (Muley, 2014; Rao & Kalainathan, 2012; Selvapandiyan *et al.*, 2013; Bhandari *et al.*, 2014). The difference in band gap of pure ZTS may be due to a change in cutoff wavelength, and that may also depend on the quality of the crystals and lattice variation. Because there are two more absorption bands in the PRZTS crystals due to the PR dye, two more band gaps were computed. These were found to be ∼2.15 and 2.5 eV in the two dyed crystals. Owing to the high band gap, the grown crystals may be applied in electro-optic devices (Periyasamy *et al.*, 2007; Shkir, Riscob *et al.*, 2014).

3.6. Photoluminescence analysis

Figs. 7(*a*) and 7(*b*) show the measured PL emission spectra for the ZTS and PRZTS single crystals at 300 K. The two excitation wavelengths $\lambda_{exc} = 310$ and 385 nm were used to record the emission spectra of each of the crystals. The 310 nm PL spectra of ZTS and 1 and 2 wt% PR-dyed ZTS crystals have a UV emission band at ∼368, 361 and 361 nm, respectively, with enhanced PL intensity and a slight shift in peak position for the dyed crystals. A violet–blue emission band is also observed at 430 nm in the pure crystals, which becomes very broad in the dyed crystals and seems to disappear. There is a new broad green emission band at ∼520 nm in the dyed crystals.

However, when the grown crystals were excited at ∼385 nm then a violet–blue emission band at 447 nm was observed for pure and dyed crystals, as shown in Fig. 6(*b*). The PL intensity of this band was enhanced with increasing dye content. The emission bands at ∼430 in pure and 447 in dyed crystals may be due to S^{2-} vacancies (Bhandari *et al.*, 2014; Kushwaha *et al.*, 2011, 2014; Rao & Kalainathan, 2012) in the ZTS crystals.

Two more emission bands are also observed, at ∼525 nm (intense) and 575 nm (broad), in the dyed crystals. These extra bands may be due to interaction of the PR dye with ZTS. Such a band for pure PR dye is reported at 545 nm when excited at 350 nm (Zarei & Ghazanchayi, 2016). The intense emission band at ∼578 nm was also reported in phenol red as fluorophore in a poly(vinyl alcohol) membrane matrix when excited at 386 nm (Zarei & Ghazanchayi, 2016). The bands are shifted to some extent and several new bands occurred in dyed ZTS crystals. These PL results suggest that the PR dye is strongly interacting with the ZTS matrix.

3.7. Dielectric and a.c. electrical conductivity analyses

For dielectric studies, the capacitance (C), impedance (Z) and loss tangent ($\tan\delta$) were measured in the frequency range from 3 kHz to 10 MHz. The dielectric constant (ε_1) and loss (ε_2) were evaluated using the well known relations given below (Kaygili *et al.*, 2013, 2015):

$$\varepsilon_1 = \frac{Cd}{\varepsilon_0 A}, \tag{1}$$

$$\varepsilon_2 = \varepsilon_1 \tan\delta, \tag{2}$$

where ε_0 is the permittivity of free space (ε_0 = 8.854 × 10^{-12} F m^{-1}), d and A are the thickness and area of the crystal sample.

Fig. 8(*a*) shows a plot of the variation of the relative permittivity (ε_1) values as a function of frequency for all the ZTS and 1 and 2 wt%-dyed PRZTS crystals. It is apparent that ε_1 is dependent on frequency in all of the crystals. The value of ε_1 is found to be almost stable in the whole tested frequency range, as we have performed this measurement in the higher frequency range. It can also be seen from Fig. 8(*a*) that ε_1 is increased in the dyed crystals from ∼12 to ∼26, which is higher than the previously reported value (Bhandari *et al.*,

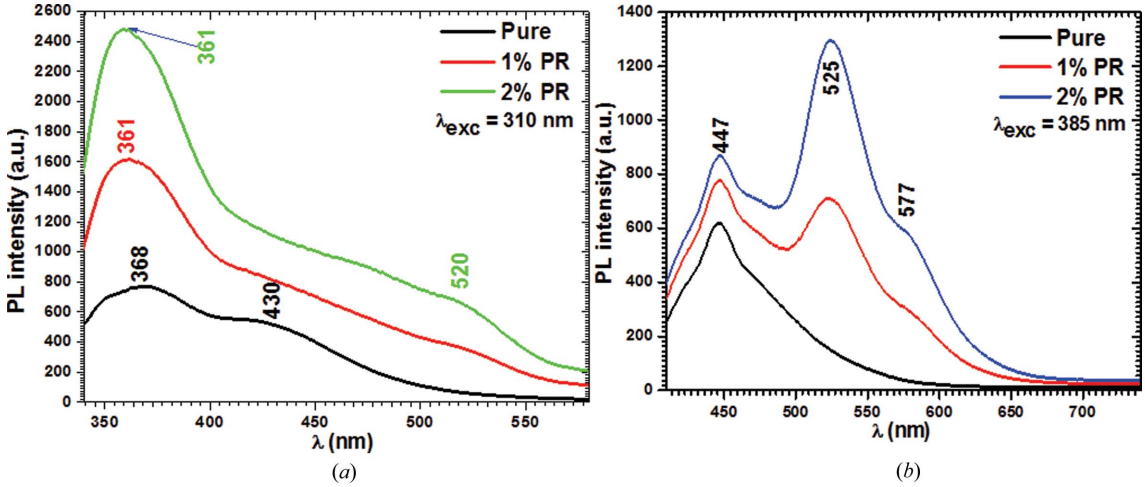

Figure 7
PL emission spectra for grown crystals excited at (*a*) 310 nm and (*b*) 385 nm.

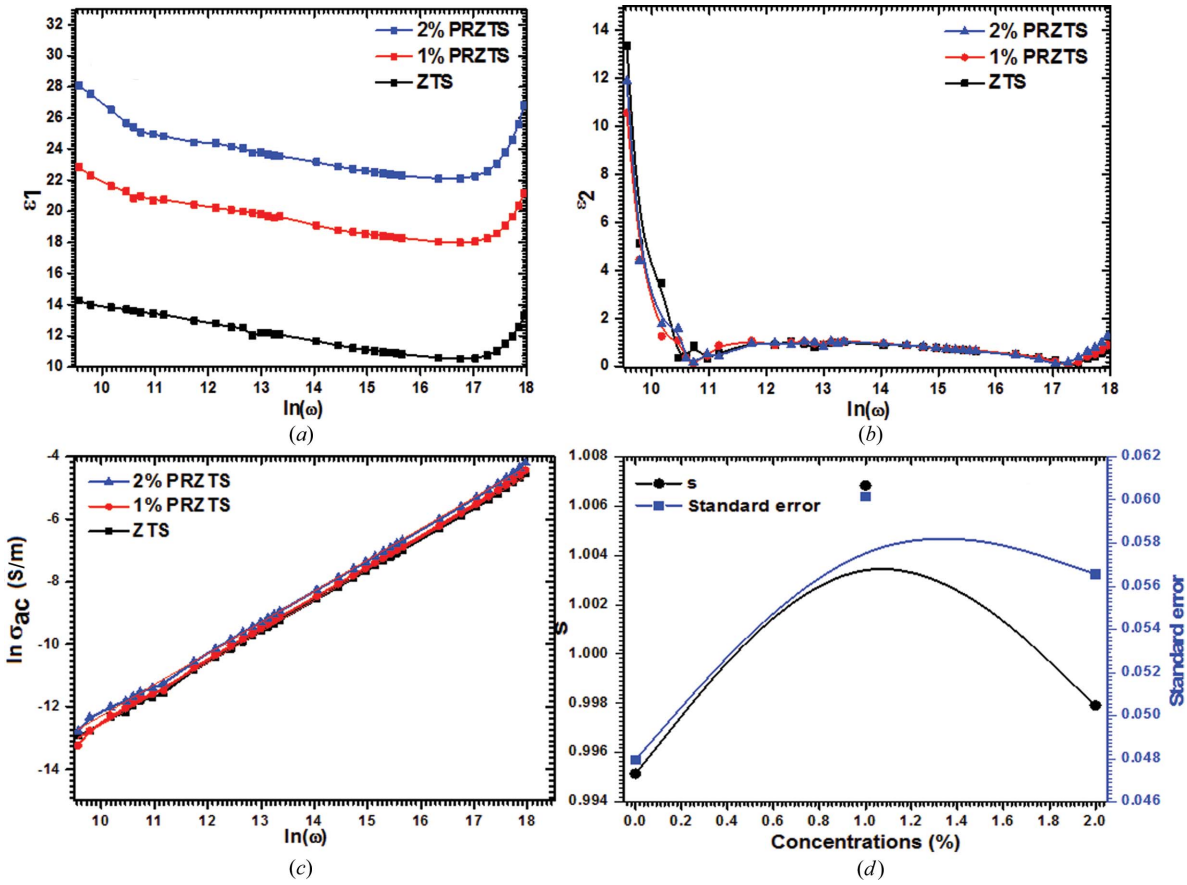

Figure 8
Plots of variation of (*a*) ε_1, (*b*) ε_2, (*c*) $\ln\sigma_{ac}$ and (*d*) s for ZTS and PRZTS crystals.

2014). Such enhancement in dyed crystals may be due to the high dielectric polarization of the added dye. The ε_2 values show similar behavior to ε_1, as shown in Fig. 8(*b*), and the low values confirm that the grown crystals contain few defects.

Furthermore, the total a.c. electrical conductivity ($\sigma_{tot.ac}$) value was calculated using the following relations (Kaygili *et al.*, 2013, 2015):

$$\sigma_{tot.ac} = \frac{d}{ZA}, \tag{3}$$

$$\sigma_{tot.ac} = \sigma_{dc} + B\omega^{s}. \tag{4}$$

Here, σ_{dc} is the direct current conductivity, B is a constant, ω is the angular frequency and s is the frequency exponent. Fig. 8(*c*) shows a plot of the variation of the total a.c. electrical conductivity with frequency. An increase in the value of $\ln\sigma_{ac}$ is observed with increasing frequency in the grown crystals, following the universal power law. The frequency exponent (s) value was also determined from the slope of the linear part of the $\ln\sigma_{ac}$ *versus* $\ln\omega$ curve (Fig. 8*c*) and found to be between 0.99514 and 1.00684, as shown in Fig. 8(*d*). The value of s is almost equal to unity for all the tested crystals. As per the available literature the value of s for ionic conducting materials is between 0.6 and 1, but its theoretical limit is 1 (Lee *et al.*, 1991). The calculated value of s is found to be $\leq$1, which shows that the hopping mechanism of conduction in the studied material involves a translational motion with sudden carrier hopping within the grown crystals.

4. Conclusion

Large-size dyed single crystals of zinc (tris) thiourea sulfate have been grown in the presence of different concentrations of phenol red dye using a simple solution method at 300 K. The size of the grown crystals with 1 wt% dye is ~25 × 29 × 5 mm and with 2 wt% dye is ~25 × 24 × 6 mm. These crystals were grown in about 60 days. The presence of the dye was proved by a robust structural and vibrational analysis. The lattice parameters are found to be affected in the presence of the dye, but the phase was not affected. The degree of crystalline perfection of pure and PR-dyed ZTS single crystals was assessed using HRXRD and it was found that the grown single crystals have very good crystalline perfection and few defects or grain boundaries. Concentrations of <2 wt% PR dye in ZTS may yield crystals with no grain boundary, since the 2 wt% PR dye concentration has given some indication of developing grain boundaries, as shown in Fig. 5(*c*). The surface morphology was studied by SEM and found to be strongly affected by the presence of the dye. The visible change in color throughout the crystals shows that the dye is homogeneously present in ZTS crystals at higher concentrations. In pure and 1 and 2 wt%-dyed ZTS crystals a strong absorption band is observed

at 276, 274 and 272 nm, respectively. However, two more absorption bands with strong absorption values are observed at 430 ± 2 and 558 ± 2 nm in both PRZTS crystals. The value of the energy gap is found to be 4.32, 4.29 and 4.25 eV for the ZTS and PRZTS crystals, respectively. Owing to the presence of more absorption bands in ZTS crystals grown in the presence of PR dye, two more band gaps were also computed and these were found to be ∼2.15 and 2.5 eV. The PL spectra of the ZTS and PRZTS single crystals excited at 310 nm show a UV emission band at ∼368, 361 and 361 nm, respectively, with enhanced PL intensity for the dyed crystals. However, under excitation at ∼385 nm, a violet–blue emission band at ∼447 ± 2 nm with increasingly enhanced PL intensity was observed in all crystals. The enhancement of PL intensity shows the formation of defects which act as color centers. The value of the dielectric constant for ZTS crystals is improved when they are grown in the presence of dye. The mechanical strength of the crystals was also found to be improved. The enhanced properties of dyed crystals suggest that they may have broad applications in the field of linear and nonlinear optical devices.

Funding information

The authors would like to express their gratitude to the Deanship of Scientific Research, King Khalid University, Saudi Arabia, for providing financial support under project No. R.G.P. 2/3/38.

References

Andreetti, G. D., Cavalca, L. & Musatti, A. (1968). *Acta Cryst.* B**24**, 683–690.
Badan, J., Hierle, R., Perigaud, A., Zyss, J. & Williams, D. (1993). *NLO Properties of Organic Molecules and Polymeric Materials*, American Chemical Society Symposium Series. Washington, DC: American Chemical Society.
Batterman, B. W. & Cole, H. (1964). *Rev. Mod. Phys.* **36**, 681–717.
Benedict, J. B., Wallace, P. M., Reid, P. J., Jang, S. H. & Kahr, B. (2003). *Adv. Mater.* **15**, 1068–1070.
Berthois, Y., Katzenellenbogen, J. A. & Katzenellenbogen, B. S. (1986). *Proc. Natl Acad. Sci. USA*, **83**, 2496–2500.
Bhandari, S., Sinha, N., Ray, G. & Kumar, B. (2014). *Chem. Phys. Lett.* **591**, 10–15.
Cole, J. M. & Hickstein, D. D. (2013). *Phys. Rev. B*, **88**, 184105.
Dhumane, N. R., Hussaini, S. S., Dongre, V. G. & Shirsat, M. D. (2008). *Opt. Mater.* **31**, 328–332.
Kahr, B. & Gurney, R. W. (2001). *Chem. Rev.* **101**, 893–951.
Kahr, B. & Shtukenberg, A. (2016). *CrystEngComm*, **18**, 8988–8998.
Kaygili, O., Dorozhkin, S. V., Ates, T., Canan Gursoy, N., Keser, S., Yakuphanoglu, F. & Birkan Selçuk, A. (2015). *Mater. Sci. Eng. C*, **47**, 333–338.
Kaygili, O., Keser, S., Ates, T., Al-Ghamdi, A. A. & Yakuphanoglu, F. (2013). *Powder Technol.* **245**, 1–6.
Kushwaha, S. K., Maurya, K. K., Haranath, D. & Bhagavannarayana, G. (2011). *J. Appl. Cryst.* **44**, 1054–1061.
Kushwaha, S., Maurya, K., Vijayan, N., Gupta, A., Haranath, D., Kumar, B., Kanjilal, D. & Bhagavannarayana, G. (2014). *Nucl. Instrum. Methods Phys. Res. Sect. B*, **338**, 1–7.
Laugier, J. & Bochu, B. (2000). *CHECKCELL*. Laboratoire des Materiaux et du Génie Physique de l'Ecole Supérieure de Physique de Grenoble, France.
Lee, W., Liu, J. F. & Nowick, A. (1991). *Phys. Rev. Lett.* **67**, 1559–1561.
Mills, A. & Skinner, G. A. (2011). *Analyst*, **136**, 894–896.
Moitra, S. & Kar, T. (2007). *Opt. Mater.* **30**, 508–512.
Muley, G. (2014). *J. Elec Mater.* **43**, 439–446.
Penn, B. G., Cardelino, B. H., Moore, C. E., Shields, A. W. & Frazier, D. (1991). *Prog. Cryst. Growth Charact. Mater.* **22**, 19–51.
Periyasamy, B. K., Jebas, R. S. & Thailampillai, B. (2007). *Mater. Lett.* **61**, 1489–1491.
Rao, R. H. & Kalainathan, S. (2012). *Spectrochim. Acta A Mol. Biomol. Spectrosc.* **97**, 456–463.
Rovati, L., Fabbri, P., Ferrari, L. & Pilati, F. (2012). *Fiber Optic Sensors*, edited by M. Yasin, ch. 17. InTech. https://doi.org/10.5772/26517.
Saleh, B. E. A. & Teich, M. C. (1991). *Fundamentals of Photonics*, Wiley Series in Pure and Applied Optics, pp. 644-695. New York: John Wiley and Sons.
Selvapandiyan, M., Arumugam, J., Sundaramoorthi, P. & Sudhakar, S. (2013). *J. Alloys Compd.* **558**, 34–38.
Shakir, M., Kushawaha, S. K., Maurya, K. K., Kumar, S., Wahab, M. A. & Bhagavannarayana, G. (2010). *J. Appl. Cryst.* **43**, 491–497.
Shakir, M., Kushwaha, S., Maurya, K., Bhatt, R., Rashmi, Wahab, M. A. & Bhagavannarayana, G. (2010). *Mater. Chem. Phys.* **120**, 566–570.
Shakir, M., Singh, B., Kumar, B. & Bhagavannarayana, G. (2009). *Appl. Phys. Lett.* **95**, 252902.
Shkir, M. (2016). *J. Mater. Res.* **31**, 1046–1055.
Shkir, M., Abbas, H., Kumar, S., Bhagavannarayana, G. & AlFaify, S. (2014). *J. Phys. Chem. Solids*, **75**, 959–965.
Shkir, M., AlFaify, S., Abbas, H. & Bhagavannarayana, G. (2015). *Mater. Chem. Phys.* **155**, 36–46.
Shkir, M., AlFaify, S., Ganesh, V., Yahia, I., Algarni, H. & Shoukry, H. (2016). *J. Mater. Sci. Mater. Electron.* **27**, 10673–10683.
Shkir, M., Muhammad, S. & AlFaify, S. (2015). *Spectrochim. Acta A Mol. Biomol. Spectrosc.* **143**, 128–135.
Shkir, M., Muhammad, S., AlFaify, S., Irfan, A. & Yahia, I. (2015). *Spectrochim. Acta A Mol. Biomol. Spectrosc.* **137**, 432–441.
Shkir, M., Riscob, B., Hasmuddin, M., Singh, P., Ganesh, V., Wahab, M., Dieguez, E. & Bhagavannarayana, G. (2014). *Opt. Mater.* **36**, 675–681.
Ushasree, P. M., Jayavel, R. & Ramasamy, P. (1999). *Mater. Sci. Eng. B*, **65**, 153–158.
Ushasree, P., Jayavel, R., Subramanian, C. & Ramasamy, P. (1999). *J. Cryst. Growth*, **197**, 216–220.
Venkataramanan, V., Srinivasan, M. & Bhat, H. (1994). *J. Raman Spectrosc.* **25**, 805–811.
Wahab, H. S. & Hussain, A. A. (2016). *J. Nanostruct. Chem.* **6**, 261–274.
Wanke, M. C., Lehmann, O., Müller, K., Wen, Q. & Stuke, M. (1997). *Science*, **275**, 1284–1286.
Yang, S. M. & Ozin, G. A. (2000). *Chem. Commun.* pp. 2507–2508.
Zaitseva, N. & Carman, L. (2001). *Prog. Cryst. Growth Charact. Mater.* **43**, 1–118.
Zarei, A. R. & Ghazanchayi, B. (2016). *Talanta*, **150**, 162–168.